



Shaping Tumor Microenvironment by Amplifying the Complement Cascade for Improved Immune Response in Pancreatic Cancer Model

Menghan Gao¹, Sultana Kechagia¹, Mohanraj Ramachandran¹, Vivek Anand Manivel¹, Nadir Kadri², Beatrice-Ana Cicortas², Chuan Jin¹, and Di Yu¹

ABSTRACT

Antibodies against galactose- α -1,3-galactose (α Gal) are among the most abundant natural antibodies in humans and have been exploited in cancer immunotherapy, with their efficacy partly attributed to complement activation. We aim to enhance this response by employing properdin [also known as factor P (FP)], the only known positive complement regulator. We expressed a membrane-anchored properdin (mFP) on mouse and human pancreatic cancer cells and assessed its ability to enhance α Gal-mediated complement activation. We showed here that ectopic expression of mFP on Panc02 cells increased the deposition level of C3 *in vitro* and induced more potent complement-dependent cytotoxicity in the presence of human complement source. In an immunized *Ggta1* knockout mouse model, which has circulating anti- α Gal antibodies as a mimicry of the human system, mFP expression conferred significantly delayed tumor growth and was

associated with pronounced remodeling of the immune landscape in the tumor microenvironment (TME). Specifically, we observed a marked increase in conventional type 1 dendritic cells, a reduction in tumor-associated monocytes/macrophages with a shift toward a pro-inflammatory phenotype, and a transition of CD8⁺ T cells toward a progenitor-exhausted state. Reconfiguring the structure of mFP to create an artificial C3 convertase binding site and incorporating an intracellular oligomerization domain improved target cell killing and monocyte-mediated phagocytosis in a human whole-blood loop model. These findings suggest that amplifying complement activation can delay tumor growth and alter the TME in the context of a murine pancreatic cancer model. Furthermore, we have developed a novel membrane-bound oligomerized FP functional unit, which effectively elicits robust complement activation.

Introduction

Cancer immunotherapy leverages the body's own immune system to identify, attack, and eradicate cancer cells. It is a rapidly expanding field with a diverse array of innovative strategies. Approaches leveraging xenogeneic rejection mediated by pre-existing natural antibodies against galactose- α -1,3-galactose (α Gal) epitopes have been utilized for cancer immunotherapy (1–3). α Gal is a glycol modification catalyzed by glycoprotein α -1,3-galactosyltransferase (GGTA1), which is universally present on mammal cells except for humans, apes, and Old World monkeys (1). During evolution, humans lost the gene *GGTA1*, instead, humans developed a high titer of anti- α Gal antibodies, constituting approximately 1% of the total immunoglobulins (1) in the form of IgG, IgM, and IgA isotypes (4). Opsonization by anti- α Gal antibodies on tumor cells has

been indicated to initiate complement activation and lead to complement-dependent cytotoxicity (CDC) on tumor cells (5, 6).

Given the pivotal role of CDC in the targeted elimination of tumor cells mediated by monoclonal antibodies (7–9), we hypothesize that augmenting complement activation using properdin can enhance the efficacy of α Gal-based therapies. Properdin, also referred to as factor P (FP), is the only identified positive complement regulator (10, 11). FP comprises a TGF- β binding (TB) domain, followed by six thrombospondin type I repeats (TSR1–TSR6; refs. 12, 13). FP functions to stabilize convertases that participate in the alternative pathway (AP), one of the three major pathways of the complement cascade, alongside the classical pathway and the lectin pathway. By binding to C3b, FP extends the half-life of the AP C3 convertase C3bBb by up to 10-fold (14) and impedes the factor H-mediated cleavage of C3b by factor I (15–17). Under physiologic conditions, FP predominantly circulates as dimers, trimers, and tetramers in a ratio of around 1:2:1, forming a ring-shaped structure with units aligned head to tail (18, 19). The C3b-binding site of FP has been shown to localize at the connecting vertices of the ring-shaped oligomers, which are formed by the TB domain and TSR1 of one monomer, along with TSR4, TSR5, and TSR6 from an adjacent monomer (12, 20).

This study aims to employ membrane-anchored FP (mFP) to amplify the complement activation provoked by α Gal-based cancer immunotherapies. We selected pancreatic ductal adenocarcinoma as a representative model of challenging solid tumors given its rapid progression, immunosuppressive tumor microenvironment (TME), and limited response to established immunotherapies (21). Our findings indicate that mFP enhanced anti- α Gal-dependent complement activation, leading to delayed tumor growth and remodeling of the TME in the tested murine model. Through protein engineering,

¹Department of Immunology, Genetics and Pathology, Uppsala University, Uppsala, Sweden. ²Department of Laboratory Medicine, Karolinska Institute, Solna, Sweden.

C. Jin and D. Yu have shared senior authorship.

Corresponding Authors: Chuan Jin, Department of Immunology, Genetics and Pathology, Science for Life Laboratory, Uppsala University, Rudbeck Laboratory, Dag Hammarskjöldsväg 20, Uppsala 751 85, Sweden. E-mail: chuan.jin@igp.uu.se; and Di Yu, di.yu@igp.uu.se

Mol Cancer Ther 2026;25:469–79

doi: 10.1158/1535-7163.MCT-24-0898

This open access article is distributed under the Creative Commons Attribution-NonCommercial-NoDerivatives 4.0 International (CC BY-NC-ND 4.0) license.

©2025 The Authors; Published by the American Association for Cancer Research

specifically by rearranging TSR domains and incorporating an intracellular oligomerization domain, we observed improved complement activation, phagocytosis, and cancer cell cytotoxicity in a human whole-blood model.

Materials and Methods

Cell culture

The murine pancreatic cancer cell line Panc02 (RRID: CVCL_D627) and human pancreatic cell lines Panc-1 (RRID: CVCL_0480) and MiaPaca-2 (RRID: CVCL_0428) were kindly provided by Dr. Rainer Heuchel at Karolinska Institute in 2008, with the most recent short tandem repeat authentication performed in 2019. All the cells were cultured in DMEM (Gibco, #11965092) supplemented with 10% FBS (Gibco, #A5256801), 100 U/mL penicillin-streptomycin (Gibco, #15140122), and 1 mmol/L sodium pyruvate (Gibco, #11360039) in a humidified incubator (Thermo Fisher Scientific) at 37°C supplied with 5% CO₂. Cell lines were tested for *Mycoplasma* contamination before each batch of cell culture using the MycoAlert Detection Kit (Lonza, #LT07-318), and no contamination was detected. Cells were used within eight passages after thawing.

Mouse strain and immunization

All animal studies were conducted following the 3R principle and approved by the regional Uppsala Research Animal Ethics Committee (dossier number: 5.8.18-19434/2019 and 5.8.18-16015/2024).

Ggta1 knockout (KO) mice on a C57BL/6 background (22) were a kind gift from Dr. Park's lab (Seoul National University), originated from Dr. D'Apice's lab (St. Vincent's Hospital), and were maintained as an inbred strain at the animal facility of Rudbeck Laboratory, Uppsala University, Sweden. To generate anti-αGal mice, *Ggta1*-KO mice were immunized with 100 μg of mucin (Sigma-Aldrich, #M2378) and 1 μg of polyinosinic-polycytidylic acid (poly I:C; Sigma-Aldrich, #P0913) in 150 μL phosphate-buffered saline (PBS) administered on days 0 and 14 to induce the development of antibodies against αGal epitopes.

Vector design and cell engineering

To generate *Ggta1*-KO Panc02 cells, gRNA (GTTGTCTTCTTGA-TAACTGT) targeting the murine *Ggta1* gene was inserted into the pX458 plasmid (Addgene, #48138, RRID: Addgene_48138) and transfected into Panc02 cells using Lipofectamine 3000 (Invitrogen, #L3000015). Transfected cells were kept in the selective medium for 1 week, followed by cell sorting and expansion. To engineer human pancreatic cancer cells to express GGTA1, *GGTA1* coding sequence from *Sus scrofa* was ordered from GenScript and cloned into a lentiviral vector.

To generate murine mFP (muP), the original secretion signal sequence of mouse properdin [amino acid (aa) 1–23] was substituted with that from mouse IgGκ (aa 1–21). Additionally, a transmembrane helix and a truncated intracellular domain from mouse CD80 (or B7-1, aa 247–273; ref. 23) were fused to the C-terminus of mouse properdin, linked by a GS linker (GGGS). To generate human mFP (huP), the original secretion signal sequence of human properdin (aa 1–27) was substituted with that of human CD8a (aa 1–21). Additionally, a transmembrane helix from human CD8a (aa 183–206) and a cytosolic tail from human TCR-β (aa 317–325) were fused to the C-terminus of mouse properdin, linked by a GS linker (GGGS). To generate huP-1 to -6, the N-terminal (TB and TSR1-3) and C-terminal (TSR4-6) halves of FP in huP were

swapped (TSR4-TSR5-TSR6-TB-TSR1-TSR2-TSR3). huP-1 to -6 have the same secretion signal sequence and transmembrane domain as huP. huP-1 and -2 have the same cytosolic tail as huP. huP-3 and -4 have GCN4pII (24) after the transmembrane domain. huP-5 and -6 have GCN4pIL (24) after the transmembrane domain. huP-1, -3, and -5 have a shorter flexible linker (GGGS)₂ between TSR6 and TB domain. huP-2, -4, and -6 have a longer flexible linker (GGGS)₃ between TSR6 and TB domain. The aa sequences of all mFP constructs, along with their corresponding GenBank accession numbers, are provided in Supplementary Data S1.

All designed constructs for gene expression were synthesized and cloned into a third-generation self-inactivating lentiviral vector (System Biosciences) under the control of elongation factor-1α promoter by GenScript. Lentiviral particles were generated as previously described (25). Cells were transduced by adding concentrated lentiviral particles directly to the cell culture. The transduced cells were sorted using BD FACSAria III (BD Biosciences) following at least 1 week of culture after transduction.

The expression of αGal and mFP was examined by flow cytometry (Supplementary Table S1) using a CytoFLEX LX flow cytometer (Beckman Coulter).

Cell growth quantification *in vitro*

On day 0, 10,000 Panc02 or Panc02 muP cells were seeded per well in a 24-well plate. On days 1, 2, and 3, cells were detached by 0.05% trypsin-EDTA (Gibco, #25300062) and then stained with 0.4% trypan blue solution (Gibco, #15250061) for counting using a TC20 automated cell counter (Bio-Rad).

Antibody and C3 deposition assay

Cells were detached, resuspended in complement buffer [Dulbecco's phosphate-buffered saline (DPBS) with 5 mmol/L MgCl₂ and 2.5 mmol/L CaCl₂], and seeded at a concentration of 100,000 cells per 75 μL per well in an untreated 96-well plate. Subsequently, 25 μL of normal human serum (NHS) or anti-αGal mouse serum (AMS) was added to the cells. For controls, 25 μL of FBS or serum with 40 mmol/L EDTA was added to the cells instead. Cells were incubated at 37°C for 1 hour, washed twice with PBS containing 3 mmol/L EDTA, and then stained using a panel of fluorochrome-conjugated antibodies (Supplementary Table S2) diluted in Brilliant Stain Buffer Plus (BD Biosciences, #566385). Flow cytometry analysis was conducted using a CytoFLEX LX flow cytometer (Beckman Coulter).

NHS was purchased from the Blood Center at Uppsala Academic Hospital, Uppsala, Sweden. AMS was obtained from *Ggta1*-KO mice that had been immunized with mucin and poly I:C (as detailed in the previous section). Blood was drawn via cardiac puncture under anesthesia and allowed to clot at room temperature for 30 minutes. After clotting, the blood was centrifuged at 2,000 × *g* for 10 minutes to separate the serum. The serum (supernatant) was then collected and stored at –80°C until needed.

CDC assay

Cells were detached, resuspended in complement buffer (DPBS with 5 mmol/L MgCl₂ and 2.5 mmol/L CaCl₂), and plated at a concentration of 100,000 cells per 75 μL per well in an untreated 96-well plate. Subsequently, 25 μL of NHS or AMS was added to the cells. For controls, 25 μL of FBS (live control) or serum with 40 mmol/L EDTA was added instead. Cells were then incubated at 37°C for 2 hours. Separate wells were prepared in which all cells were killed using 0.1% saponin (dead control). Next, 4 μmol/L

ethidium homodimer-1, which permeates only cells with damaged membranes, was added and incubated for an additional 20 minutes at 37°C. After washing the cells twice with PBS, they were transferred to a 96-well clear-bottom plate. Fluorescence at 645 nm was measured using a CLARIOstar Microplate Reader (BMG Labtech). The percentage of dead cells was calculated using the formula $(F_{\text{sample}} - F_{\text{live ctrl}})/(F_{\text{dead ctrl}} - F_{\text{live ctrl}})\%$.

Membrane complement regulatory protein knockdown

Double-stranded siRNAs targeting CD46, CD55, and CD59 were purchased from Integrated DNA Technologies (TriFECTa RNAi Kit), with three siRNAs provided for each target. The siRNAs demonstrating better knockdown efficiency and lower cytotoxicity were selected for further use. siRNA-induced knockdown was carried out as previously described (26). For single siRNA transfections, a concentration of 10 nmol/L was used. When combining siRNAs for CD46, CD55, and CD59, either 3.3 nmol/L of each (in total 10 nmol/L) or 10 nmol/L of each (in total 30 nmol/L) siRNA was applied. The expression levels of CD46, CD55, and CD59 were quantified by flow cytometry (Supplementary Table S3) using a CytoFLEX LX flow cytometer (Beckman Coulter). Subsequent CDC experiments were then conducted.

Western blotting

Cells were harvested and lysed in RIPA Lysis and Extraction Buffer (Thermo Fisher Scientific, #89900) supplemented with a protease inhibitor cocktail (Thermo Fisher Scientific, #87786) following the manufacturer's instructions. The extracted protein concentration was determined using the Bicinchoninic Acid Protein Assay Kit (Thermo Fisher Scientific, #23225). Non-reducing LDS Sample Buffer (Thermo Fisher Scientific, #84788) was added to the samples prior to loading. Sample Reducing Agent (Invitrogen, #B0009) was also added to the reduced samples, which were then heated at 70°C for 10 minutes. Equal amounts of protein were separated by 4% to 12% Bis-Tris gels (Invitrogen, NP0323BOX) and transferred onto nitrocellulose membranes (Bio-Rad, #12990). Membranes were blocked with 5% BSA in PBS with 0.05% Tween-20 (PBS-T) for 1 hour at room temperature and then probed with primary antibodies (Supplementary Table S4) diluted in 1% BSA in PBS-T overnight at 4°C. After washing with PBS-T, membranes were incubated with horseradish peroxidase-conjugated secondary antibodies (Supplementary Table S4) diluted in 5% BSA in PBS-T for 1 hour at room temperature. Protein bands were visualized using enhanced chemiluminescence substrate (Thermo Fisher Scientific, #34580) and imaged with the iBright Imaging System (Invitrogen). GAPDH was used as a loading control.

Whole-blood loop assay

The study was conducted in full accordance with the principles of the Declaration of Helsinki and the EU General Data Protection Regulation. Ethical approval for blood collection was granted by the Swedish Ethical Review Authority (permit no. 2017/492). Written informed consent was obtained from all donors.

Panc-1 cells were detached using Accutase (Gibco, #A1110501) and stained with 10 $\mu\text{mol/L}$ pHrodo (Invitrogen, #P36600) in PBS for 10 minutes at room temperature. The cells were then washed and resuspended in PBS to a concentration of 5,000 cells/ μL .

Fresh whole blood was collected from five healthy volunteers (D1–D5) into MPC polymer (NOF, #CM5206)-coated tubes and immediately mixed with soluble heparin to a final concentration of 2 IU/mL. Then, 950 μL of blood was transferred to each 2 mL

MPC-coated tube, followed by the addition of 50 μL Panc-1 cells to each tube. PBS was used in place of blood or Panc-1 cells as negative controls. The tubes were placed on a rotating wheel (15 rpm) inside an incubator at 37°C. After 15 minutes of incubation, samples were collected and placed on ice.

Red blood cells were lysed before staining. The remaining cells were first stained with a fixable viability dye, following the manufacturer's instructions (Supplementary Table S2). To block non-specific Fc receptor binding, anti-human CD16/CD32 antibodies (BD Biosciences, #564219, RRID: AB_2728082) were used. Cells were then stained using a panel of fluorochrome-conjugated antibodies (Supplementary Table S2) diluted in Brilliant Stain Buffer Plus (BD Biosciences, #566385). Flow cytometry analysis was conducted using a CytoFLEX LX flow cytometer (Beckman Coulter). The percentage of killed cancer cells was calculated as the difference between the percentage of dead Panc-1 cells in blood and PBS. Monocytes and neutrophils that performed phagocytosis were gated based on control samples from blood incubated with PBS.

Animal studies

For evaluating the growth of Panc02 wild-type (WT; G^+muP^-) or Panc02 muP (G^+muP^+) cells *in vivo* in the absence of anti- αGal effect, each male *Ggta1*-KO mouse, 6 to 8 weeks old, was inoculated subcutaneously with 20,000 tumor cells (suspended in 100 μL of sterile DPBS) into the right hind flank. For evaluating the growth of Panc02 WT (G^+muP^-) or Panc02 muP (G^+muP^+) cells *in vivo* in the presence of anti- αGal effect, male *Ggta1*-KO mice, 6 to 8 weeks old, were immunized with mucin and poly I:C as described in the previous section. Seven days after the second vaccination, each mouse was inoculated subcutaneously with 20,000 tumor cells suspended in 100 μL of sterile DPBS into the right hind flank. Tumor growth was monitored every 2 or 3 days using calipers, and tumor volume was calculated using the formula $\text{volume} = \text{length} \times \text{width} \times \text{width} \times \pi/6$. Mice were sacrificed when tumors reached a maximum volume of 500 mm^3 or if they developed non-healing ulcers or signs of distress, in accordance with ethical guidelines.

To analyze tumor-infiltrating leukocytes, tumors were harvested 18 days after implantation. The tumor fragments were enzymatically digested using Liberase TL (Roche, #05401020001) at a concentration of 12.5 $\mu\text{g/mL}$ in 2 mL of RPMI-1640 medium (Gibco, #11875093). The digestion was performed at 37°C for 30 minutes. After digestion, the tumor tissue was filtered through a 70- μm cell strainer.

Red blood cells were lysed before staining. The remaining cells were first stained with a fixable viability dye, as per the manufacturer's instructions (Supplementary Table S5). To block nonspecific Fc receptor binding, anti-mouse CD16/CD32 antibodies (BD Biosciences, #553142, RRID: AB_394657) were used. Cells were then stained with a panel of fluorochrome-conjugated antibodies (Supplementary Table S5) diluted in Brilliant Stain Buffer Plus (BD Biosciences, #566385). Intracellular or intranuclear markers were stained using eBioscience Foxp3/Transcription Factor Staining Buffer Set (Invitrogen, # 00-5523-00) according to the manufacturer's protocol. Flow cytometry analysis was performed using a CytoFLEX LX flow cytometer (Beckman Coulter).

Data analysis

Flow cytometry data were processed using FlowJo (version 10.10, FlowJo LLC, RRID: SCR_008520). All statistical analyses were performed using GraphPad Prism (version 10, GraphPad Software, RRID: SCR_002798). The normality of the data was assessed using

the Shapiro–Wilk test. Comparisons between two groups were conducted using an unpaired two-tailed Student *t* test. For analyses involving more than two groups, one-way or two-way ANOVA, followed by Tukey multiple comparisons, was used. Specifically, for whole-blood loop assay, differences between groups were analyzed using a paired (donor-matched) one-way ANOVA with Geisser–Greenhouse correction, followed by a Tukey multiple comparison test. Survival curve statistics were performed using the log-rank test. Statistical significance was set at $P < 0.05$. Further details on the statistical analyses can be found within the figure legends.

Results

Murine recombinant mFP enhanced complement activation induced by α Gal epitope on cancer cells

The α Gal epitope is widely present in non-primate mammals (1), including mice. We confirmed the retention of α Gal epitopes after cancerous transformation on the murine pancreatic cancer cell line Panc02 by flow cytometry analysis (Supplementary Fig. S1A). The expression of α Gal epitopes on Panc02 elicited opsonization by IgG (Supplementary Fig. S1B) and activation of complement on the cell surface, as evidenced by the deposition of C3, the central player in the complement cascade (Supplementary Fig. S1C and S1D). To enrich FP on the cancer cell surface, we developed an mFP by fusing murine FP with the transmembrane domain and the truncated cytosolic tail of murine CD80, termed muP (Fig. 1A; Supplementary Data S1). To determine the potential of muP to enhance

complement activation, we genetically modified Panc02 cells to express muP. The surface expression of muP was confirmed by flow cytometry (Fig. 1B). We then assessed whether muP could enhance the complement activation induced by α Gal. *Ggta1*-KO Panc02 lacking α Gal (G^- ; Supplementary Fig. S1A), WT Panc02 (G^+ muP $^-$), and Panc02-expressing muP (G^+ muP $^+$) were incubated with anti- α Gal murine serum (AMS), and C3 deposition level was then measured. Notably, the expression of muP significantly augmented C3 deposition (Fig. 1C and D). Nevertheless, this accumulation of C3 was insufficient to induce CDC when incubated with AMS (Fig. 1E). In contrast, significant CDC was detected upon incubation with NHS, and muP sufficiently amplified the CDC induced by α Gal (Fig. 1F). This difference may be due to the generally higher efficacy of human complement compared with murine *in vitro* (27, 28). Taken together, these findings suggest that ectopic expression of muP can enhance complement activation elicited by antibody opsonization on murine cancer cells, while CDC is not fully executed.

muP delayed tumor growth and altered the immune composition of the TME

Given the significant enhancement of complement activation by mFP *in vitro*, we explored its therapeutic potential in a syngeneic murine model. Immunocompetent *Ggta1*-KO C57BL/6 mice were first immunized to generate anti- α Gal antibodies to mimic the human situation. Subsequently, Panc02 WT (G^+ muP $^-$) and Panc02 muP (G^+ muP $^+$) were implanted subcutaneously, with subsequent

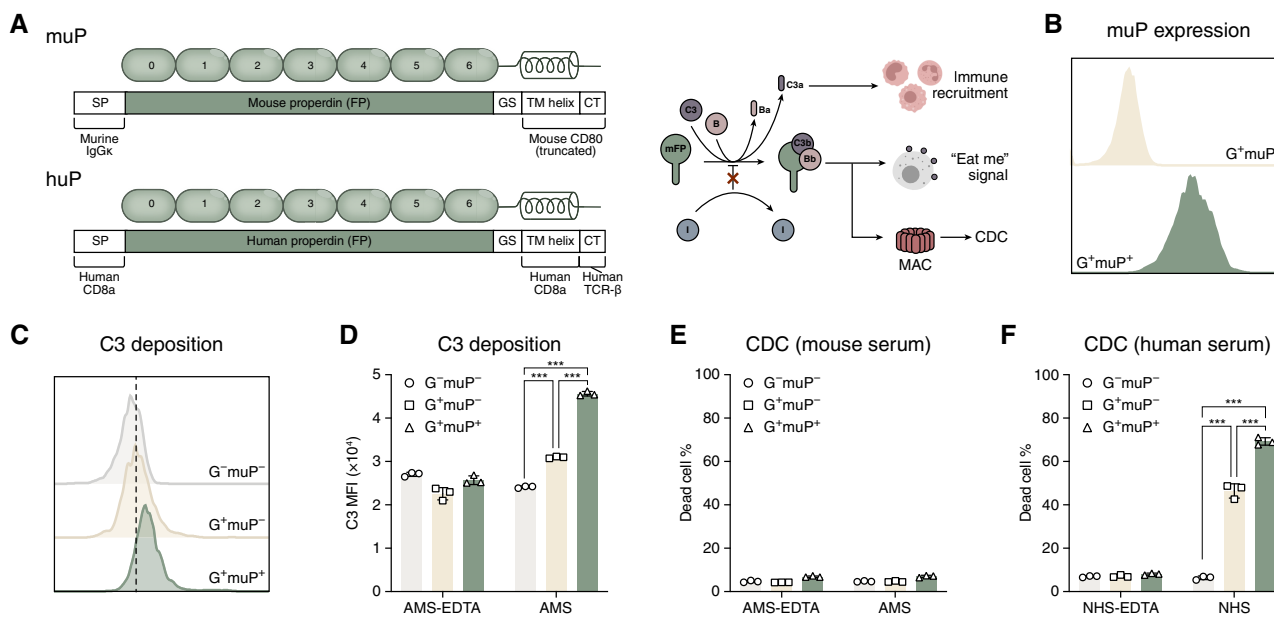


Figure 1.

muP augmented complement activation triggered by the α Gal epitope. **A**, Schematic illustration of muP and huP constructs and their proposed modes of action. CT, cytosolic tail; MAC, membrane attack complex; SP, signal peptide; TM, transmembrane. **B**, Representative histogram showing muP expression on the engineered murine pancreatic cancer cell line Panc02. **C** and **D**, C3 deposition on engineered Panc02 cell lines after 1-hour incubation with 25% AMS. EDTA (10 mmol/L) was added to the reaction to inactivate the complement as control. Data are presented in a representative histogram (**C**) and a bar plot (**D**) showing the mean fluorescence intensity (MFI) of technical triplicates with mean \pm SD from one experiment, which was repeated at least twice. **E** and **F**, CDC in engineered Panc02 cells after 2-hour incubation with 25% AMS (**E**) or 25% NHS (**F**). EDTA (10 mmol/L) was added to the reaction to inactivate the complement as control. Dead cell percentages are presented as technical triplicates with mean \pm SD from one experiment, which was repeated at least twice. The difference between groups was analyzed with one-way ANOVA, followed by a Tukey multiple comparison test. Key to statistics: ***, $P < 0.001$.

monitoring of tumor growth (Fig. 2A). Although Panc02 muP showed a similar growth rate to Panc02 WT both *in vitro* and in unvaccinated mice (Supplementary Fig. S2), it exhibited a slower growth rate in the vaccinated *Ggta1*-KO mice (Fig. 2B), leading to a significant improvement in survival (Fig. 2C). These data suggest that complement activation enhanced by muP contributes to delayed tumor growth in an anti- α Gal-dependent manner.

To gain a deeper insight into the mechanism driving the therapeutic efficacy of muP, tumor-infiltrating CD45⁺ cells were collected on day 18 after implantation for analysis of the TME by flow cytometry. We did not observe a significant difference in the percentages of myeloid cells (Fig. 2D) and T cells (Fig. 2E) within the total tumor-infiltrating leukocytes between G^+muP^- and G^+muP^+ tumors. However, a marked shift in myeloid cell

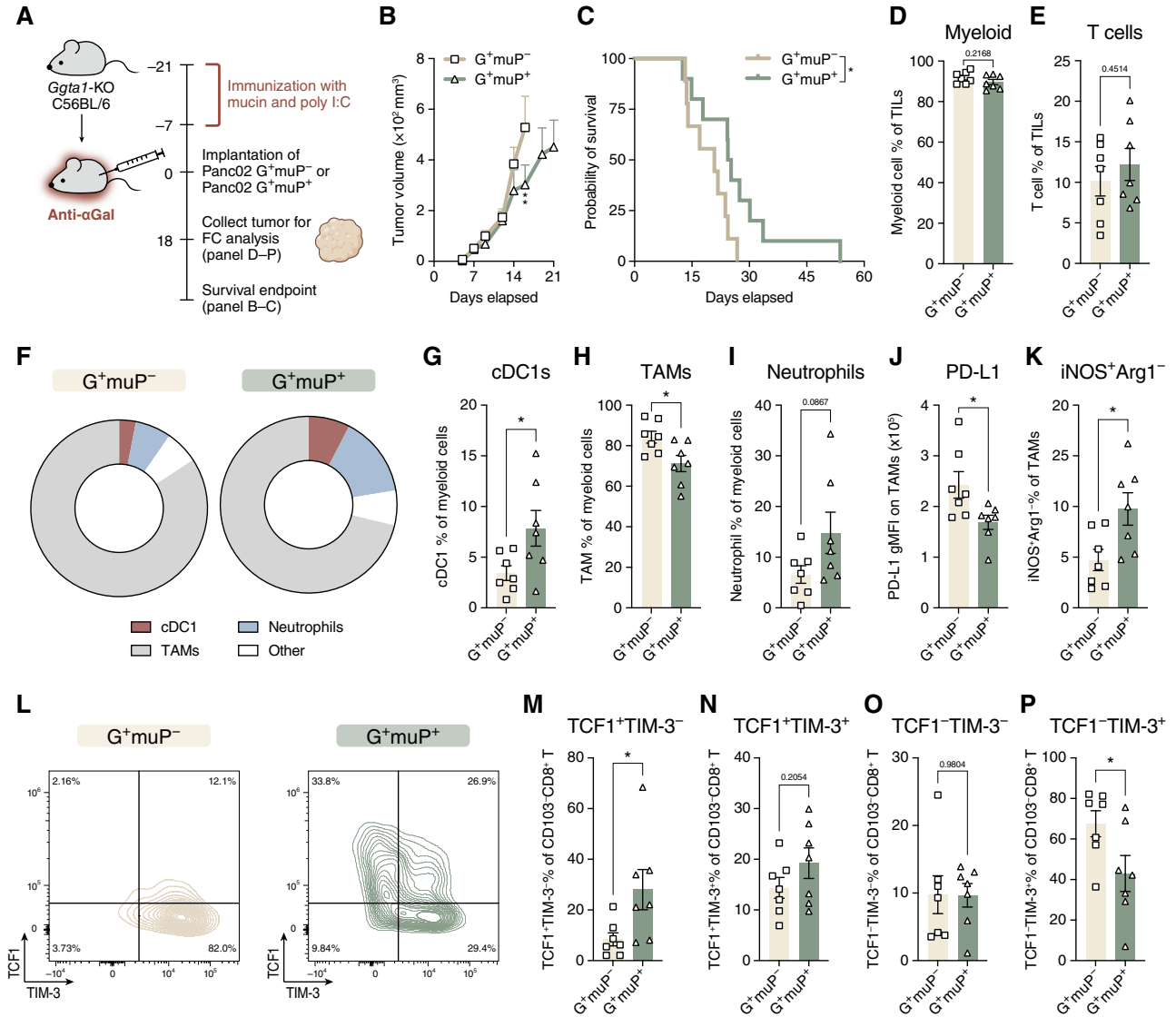


Figure 2.

Ectopic expression of muP on the cell surface delayed tumor growth and reshaped the TME. **A**, Schematic overview of the animal experiment plan. FC, flow cytometry. **B**, Tumor growth (mean \pm SEM) of Panc02 G^+muP^- ($n = 9$) and Panc02 G^+muP^+ ($n = 10$). The growth curves were compared using two-way ANOVA, followed by a Tukey multiple comparison test. **C**, Kaplan-Meier survival curve of mice implanted with Panc02 G^+muP^- ($n = 9$) or Panc02 G^+muP^+ ($n = 10$). Survival curves were compared using the log-rank test. **D-P**, Flow cytometry analysis of tumor-infiltrating immune cells from Panc02 G^+muP^- ($n = 7$) or Panc02 G^+muP^+ ($n = 7$) tumors. Gating strategies are presented in Supplementary Fig. S3. The difference between groups was analyzed using a two-tailed Student *t* test. Data are presented as individual values from each mouse with mean \pm SEM. **D** and **E**, The percentages of **(D)** myeloid cells (CD11b⁺ or CD11c⁺) and **(E)** T cells (CD3⁺) of the total tumor-infiltrating leukocytes (TILs; CD45⁺). **F-I**, Pie charts **(F)** of the distribution and the quantification of the percentages of **(G)** cDC1s (CD11b⁻CD11c⁺), **(H)** TAMs (CD11b⁺F4/80⁺ or CD11b⁺Ly6C⁺), and **(I)** neutrophils (CD11b⁺Ly6G⁺) within total myeloid cells. **J**, The geometric mean fluorescence intensity (gMFI) of PD-L1 on TAMs. **K**, Quantification of the percentages of iNOS⁺Arginase1 (Arg1)⁻ cells within TAMs. **L-P**, Representative counter plots **(L)** of TCF1 vs. TIM-3 expression on CD103⁺CD8⁺ T cells and the quantification of the percentages of **(M)** TCF1⁺TIM-3⁻ cells, **(N)** TCF1⁺TIM-3⁺ cells, **(O)** TCF1⁻TIM-3⁻ cells, and **(P)** TCF1⁻TIM-3⁺ cells within CD103⁺CD8⁺ T cells. Key to statistics: *, $P < 0.05$.

composition was noted (Fig. 2F). In G^+muP^+ tumors, there was a significant increase of conventional type 1 dendritic cells (cDC1s; Fig. 2G), accompanied by a reduction in tumor-associated monocytes/macrophages (TAMs; Fig. 2H), as well as a trend toward elevated neutrophil infiltration (Fig. 2I). Among TAMs in these tumors, PD-L1 expression was reduced (Fig. 2J), and the proportion of $iNOS^+Arginase-1^-$ TAMs was higher compared with that in G^+muP^- tumors (Fig. 2K). This $iNOS^+Arginase-1^-$ subset showed higher levels of CD86 and MHC class II, alongside lower PD-L1 expression in comparison with other subsets of TAMs (Supplementary Fig. S3E), indicative of a more pro-inflammatory phenotype.

Besides the pro-inflammatory reprogramming of myeloid cells, T cells in G^+muP^+ tumors exhibited a shift in their exhaustion state, favoring a more proliferative, progenitor-exhausted phenotype ($TCF1^+TIM-3^-$, evidenced by higher levels of Ki67 and lower levels of CD39, PD-1, and CD25) over terminal exhaustion ($TCF1^+TIM-3^+$, evidenced by lower levels of Ki67 and higher levels of CD39, PD-1, and CD25; Fig. 2L–P; Supplementary Fig. S3J). Meanwhile, no changes were observed in the ratio of $CD8^+$ to $CD4^+$ T cells, the percentages of $CD8^+$ tissue-resident memory cells ($CD103^+$), or the percentages of regulatory T cells ($Foxp3^+CD25^+$; Supplementary Fig. S3G–S3I).

Taken together, these findings suggest that the ectopic expression of muP can inhibit tumor growth, likely through alterations in the suppressed TME in the murine pancreatic cancer model.

huP is inadequate to overcome the regulation of complement negative regulators

To validate our concept in the human system, we genetically modified two human pancreatic cancer cell lines, Panc-1 and MiaPaca-2, to express GGTA1 (Supplementary Fig. S1A) and human recombinant mFP. The huP, similar to muP, is constructed by fusing FP with the transmembrane domain of human CD8a and the cytosolic tail of human TCR- β , designated as huP (Fig. 1A; Supplementary Data S1). Surface huP expression was confirmed (Fig. 3A), and its ability to augment the complement activation induced by α Gal was assessed. Contrary to the observed augmentation of C3 deposition on murine cells, the introduction of huP failed to amplify the C3 deposition induced by α Gal on human pancreatic cancer cell lines (Fig. 3B and C), probably because of a high C3 deposition that had already been elicited by α Gal antibody deposition (Supplementary Fig. S1B–S1D). Besides, CDC was not observed in either engineered Panc-1 or MiaPaca-2 when incubated with human serum (Fig. 3D). We then asked whether the ceased activation effect of huP in the context of human pancreatic cancer is attributed to the presence of negative complement regulators. As membrane complement regulatory proteins (mCRPs) CD46, CD55, and CD59 are the critical regulators that shield cells from complement attacks (29, 30), we proceeded to conduct CDC assays following the successful knockdown of CD46, CD55, and/or CD59 using siRNAs (Supplementary Fig. S4A). Knocking down either CD46 or CD55 did not sensitize the cells to CDC. However, knocking down CD59 noticeably promoted the lysis of cells expressing α Gal epitopes, and the presence of huP significantly enhanced cell lysis (Fig. 3E; Supplementary Fig. S4B). Taken together, these results indicate that CD59 is the major inhibitor that blocks the complement activation induced by α Gal and huP. In the context of human pancreatic cancer, huP is inadequate in driving

forward the complement cascade against negative regulators *in vitro*.

Rearranged huP increased cell cytotoxicity in a whole-blood loop system

The preceding results led us to improve the functionality of huP via a new conformational design. FP natively exists in dimer, trimer, or tetramer (18). The convertase-binding site of FP is typically formed by the N-terminal end (TB domain and TSR1) of one monomer and the C-terminal end (TSR4, TSR5, and TSR6) from another adjacent monomer (12, 20). Tetrameric FP was shown to have the highest activity among other oligomeric states, following the order tetramer > trimer > dimer > higher-order oligomers (18), although the underlying mechanism remains unclear. However, the oligomeric state of huP and its stereotactic conformation displayed on the cell surface remain uncertain as the huP construct was created by directly linking an FP monomer to a transmembrane domain. We therefore swapped the N-terminal and C-terminal halves of FP to artificially assemble the convertase-binding vertex found in FP oligomers. Additionally, intracellular oligomerization domains were incorporated to facilitate the multimerization of huP on the cell surface. In total, six constructs were generated with varying linker lengths and intracellular domains, named huP-1 to -6 (Fig. 4A; Supplementary Data S1). huP-1, -3, and -5 have a shorter flexible linker (GGGGS)₂, whereas huP-2, -4, and -6 have a longer flexible linker (GGGGS)₃. huP-1 and -2 only have a transmembrane domain and a short cytosolic tail, like the original huP. huP-3 and -4 have a widely used trimeric adapter GCN4pII (24), following the transmembrane helix, whereas huP-5 and -6 have GCN4pIL (24), a mutant of GCN4pII, which is prone to form tetramers.

Panc-1 was engineered to express each of these six new huP constructs, and the expression of new huP was detected by flow cytometry. Constructs huP-3, -4, -5, and -6 showed a higher expression than huP-1 and -2 (Fig. 4B). Oligomeric huP was detected from the cell lysate of Panc-1 huP-3, -4, -5, and -6 by Western blotting (Supplementary Fig. S5). C3 deposition assay was then performed on Panc-1 (G^-) expressing new huPs to screen out the best construct. huP-3, -4, -5, and -6 notably elicited elevated C3 deposition on the cell surface, whereas huP-1 and -2 exhibited much lower activity (Fig. 4C). As no clear difference was observed among huP-3, -4, -5, and -6, we proceeded with huP-3, the shortest variant with a more widely utilized oligomerization domain pII, for further investigation. Panc-1 GGTA1 cells were then modified to express huP-3 (G^+huP-3^+), followed by assessment of the capability of huP-3 to enhance complement activation triggered by α Gal. Encouragingly, significantly elevated C3 deposition was noted after the introduction of re-engineered huP on the cell surface compared with the original construct (Fig. 4D and E).

Given the challenges in assessing human complement activation and CDC in murine models, we employed a whole-blood loop assay (31) to evaluate whether the newly designed huP could improve target cancer cell killing and phagocytosis, for which cancer cells were incubated with fresh whole blood with intact complement system (Fig. 4F). Samples were collected following a 15-minute incubation for flow cytometry analysis. Notably, huP-3 induced significantly enhanced cancer cell killing and monocyte-mediated phagocytosis compared with huP despite substantial inter-donor variability (Fig. 4G–J; Supplementary Fig. S6A and S6B). However, the improvement in neutrophil-mediated

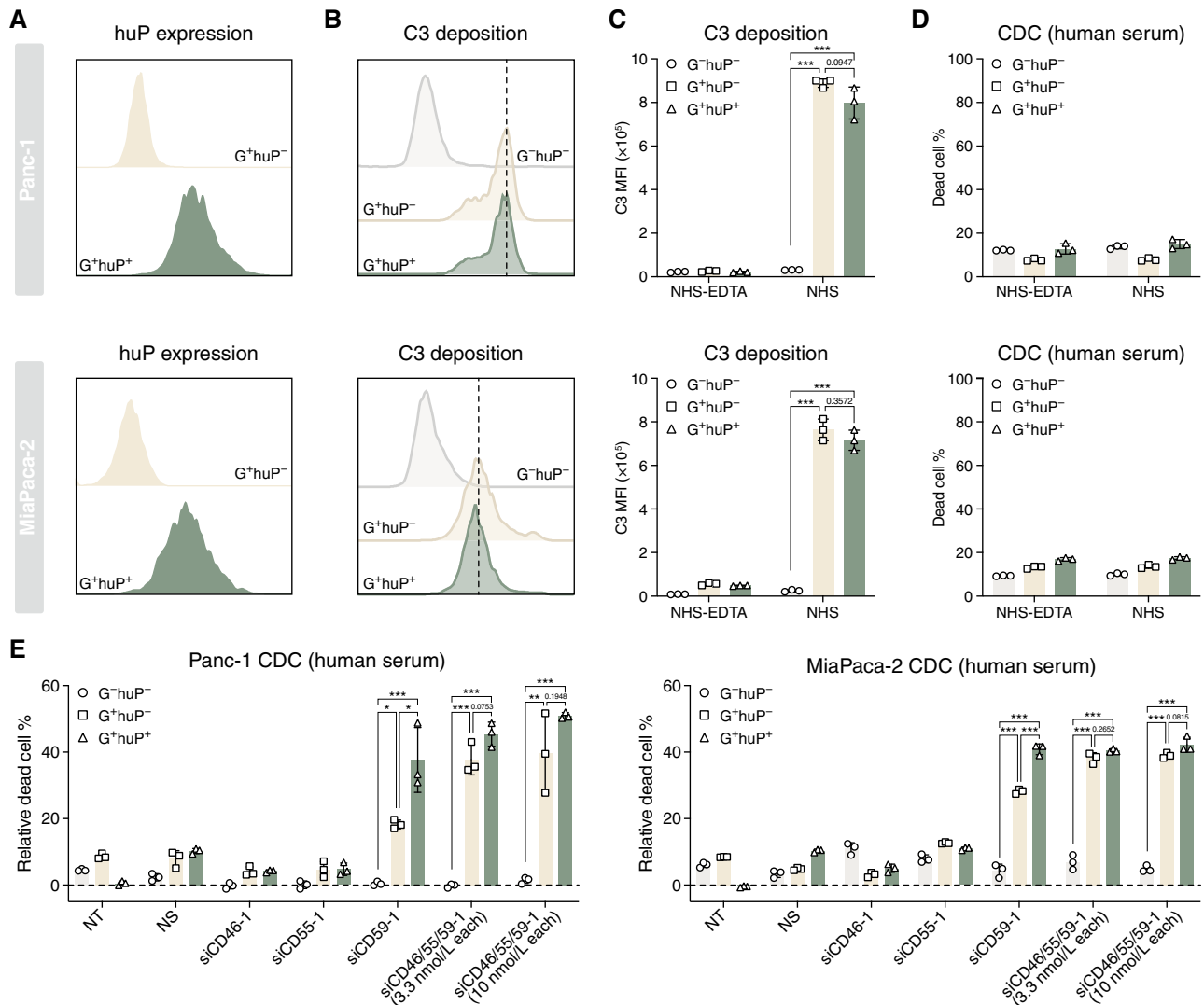


Figure 3.

The functionality of huP was hindered by membrane complement regulators. **A**, Representative histograms showing huP expression on the engineered GGTA1-expressing (G⁺) human pancreatic cancer cell lines Panc-1 and MiaPaca-2. **B** and **C**, C3 deposition on Panc-1 and MiaPaca-2 cells after 1-hour incubation with 25% NHS. EDTA (10 mmol/L) was added to the reaction to inactivate the complement as control. Data are presented in a representative histogram (**B**) and a bar plot (**C**) showing the individual mean fluorescence intensity (MFI) of technical triplicates with mean \pm SD from one experiment, which was repeated at least twice. **D**, CDC in Panc-1 and MiaPaca-2 cells after 2-hour incubation with 25% NHS. EDTA (10 mmol/L) was added to the reaction to inactivate the complement as control. Dead cell percentages are presented as technical triplicates with mean \pm SD from one experiment, which was repeated at least twice. **E**, CDC in Panc-1 and MiaPaca-2 cells after knocking down membrane complement regulators. Cells were incubated with 25% NHS in complement buffer for 2 hours. Dead cell percentages are presented as technical triplicates with mean \pm SD from one experiment, which was repeated once. NS, nonsense control; NT, non-transfected control. The difference between groups was compared using one-way ANOVA followed by a Tukey multiple comparison test. Key to statistics: *, $P < 0.05$; **, $P < 0.01$, and ***, $P < 0.001$.

phagocytosis was minor (**Fig. 4K** and **L**; Supplementary Fig. S6C). These data suggested that re-engineered huP further improves complement activation elicited by α Gal, leading to improved target cell killing and monocyte-mediated phagocytosis.

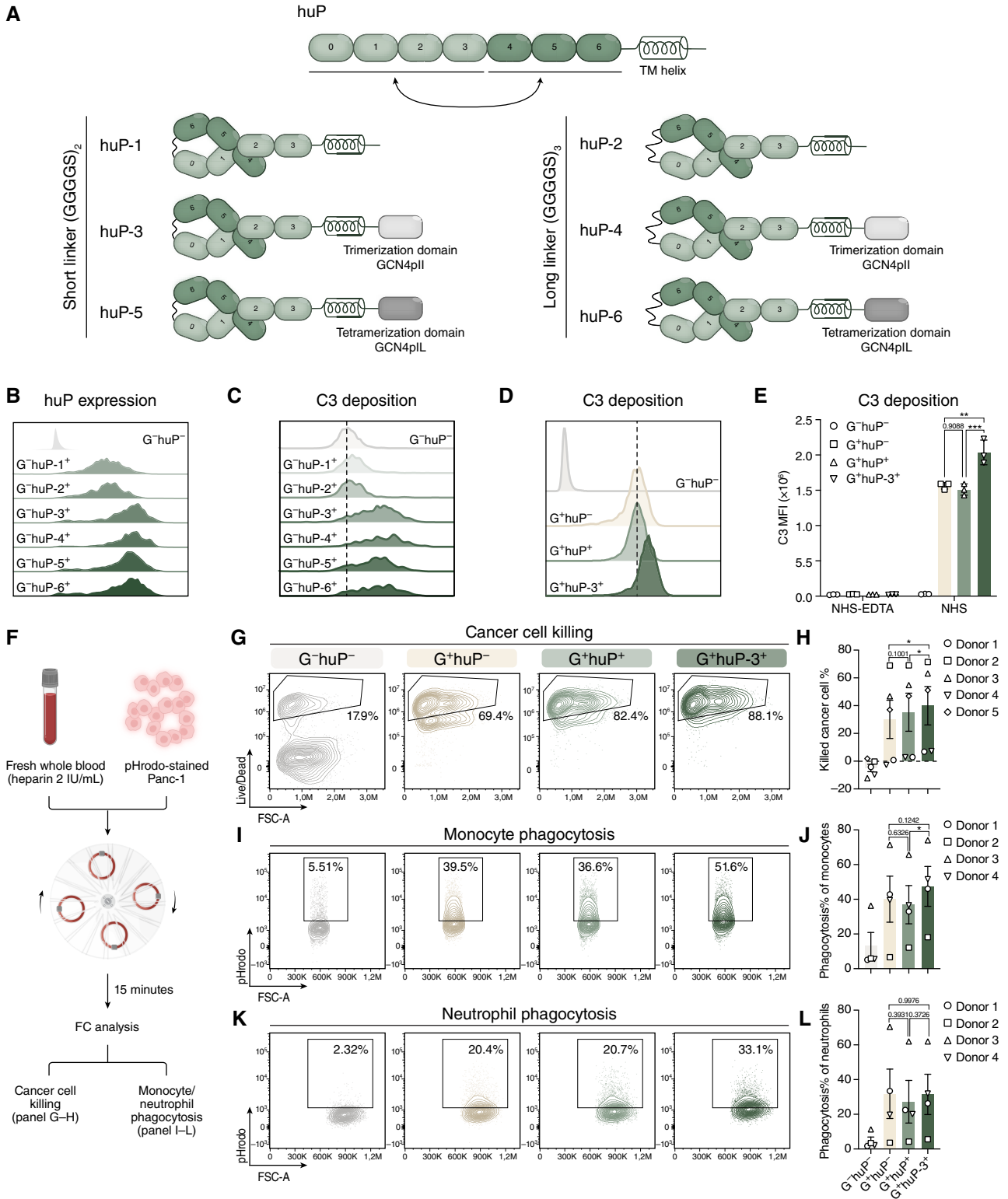
Discussion

The action of complement in the TME is highly diverse and context specific (32). Lately, there has been accumulating evidence suggesting that the depletion of different complement components

holds therapeutic potential in rodent models (9, 32). However, in the context of antibody-based immunotherapies (e.g., rituximab and daratumumab), the clinical benefits are partially explained by the induction of CDC, with the complement cascade typically retaining its role as a tumor-destructive effector (9). Similarly, α Gal-mediated immunotherapies, which utilize xenogeneic rejection, rely on antibody-dependent cytotoxicity and CDC. We hypothesize that strengthening complement activation could further improve the therapeutic potential of strategies leveraging xenogeneic rejection.

Properdin stands out as the prime candidate for amplifying complement activation as it is the only identified positive regulator of the complement system. Vuagnat and colleagues (33)

initially proposed the concept of a transmembrane recombinant FP, consisting of human FP fused with the transmembrane domain of the human platelet-derived growth factor receptor, to



Downloaded from <http://aacrjournals.org/mct/article-pdf/25/3/469/3743701/mct-24-0898.pdf> by Uppsala University user on 16 March 2026

eradicate pathogens and tumor cells by inducing AP activation directly on the cell surface. Pedersen and colleagues (34) recruited endogenous FP to the cancer cell surface by bispecific nanobodies, which induced sufficient AP activation. Nonetheless, despite the robust activation of the AP, it did not culminate in CDC, possibly because of the high expression of mCRPs on the cancer cells (34). On the other hand, the comprehensive impact of FP-induced AP activation, as well as its potential effects in combination with antibody-based therapies on modulating antitumor immunity, remains unexplored.

Here, we presented an enhanced antitumor response in the pancreatic cancer model by amplifying complement activation induced by α Gal-mediated xenogeneic rejection. Through overexpressing a recombinant membrane-bound FP (muP), we successfully induced C3 deposition on the surface of murine PDAC Panc02 cells and demonstrated improved cell death via CDC induction using human serum.

Chronic complement activation is widely regarded as protumoral, often linked to the recruitment of immunosuppressive cells and the suppression of effector cell function (9, 32, 35). In contrast, our data suggest that enhanced complement activation can be utilized to combat cancer. In the *in vivo* murine model vaccinated against α Gal, adding muP significantly delayed tumor growth, which may result from both enhanced CDC and alterations in the immune landscape of the TME. The amplified complement activation by muP led to the enrichment of cDC1s and reprogramming of TAMs toward an immunostimulatory phenotype that supports antitumor immunity (36–38). These effects may result from the intensified complement cascade, which generates a pro-inflammatory milieu through the production of cleaved complement components such as C3a and C5a (39). Moreover, increased complement deposition may promote tumor antigen uptake by antigen-presenting cells (9), enhancing antigen presentation and subsequent T-cell priming (40, 41). In the T-cell compartment, we observed a shift in CD8⁺ T cells from a more terminally exhausted toward a progenitor-exhausted phenotype, which retains proliferative capacity, replenishes the pool of cytotoxic effectors (42, 43), and has been associated with improved prognosis across multiple cancer types (44–47). This phenotypic reprogramming may be driven by the enriched dendritic cells, which facilitate maintaining the stemness of tumor-infiltrating CD8⁺ T cells (48). The reduction of TAMs may also contribute to T-cell reprogramming as antigen presentation by TAMs has been implicated in driving T-cell

exhaustion (49). Moreover, a direct contribution of complement activation to T-cell reprogramming cannot be excluded. However, the role of complement components in shaping the T-cell exhaustion trajectory remains poorly understood and requires further studies.

As we validated the concept in human cell lines, we found that introducing the xenogeneic α Gal epitope already achieved high complement activation. The enhancement by adding huP to α Gal-expressing cells is therefore marginal. The lack of CDC is also confirmed because of the presence of high levels of mCRPs on the cancer cell membrane. The activity of FP is affected by its oligomerization states (18). Among the physiologic oligomeric forms of FP (dimer, trimer, and tetramer), tetrameric FP exhibits the highest activity (18). A vertex containing the binding site for C3b (50) can be isolated while preserving its activity, albeit with lower activity compared with the native oligomeric FP (13). By relocating TSR4 to TSR6 over the TB domain, we artificially congregate the key components for assembling the C3b-binding domain, mimicking the structure of a cleaved vertex, and the activity of the rearranged huP can be amplified by incorporating an intracellular oligomerization domain. Complement activation can elicit effects beyond CDC, as the deposition and release of complement components have a complex impact on immune responses. We therefore assessed the functionality of the rearranged huP in a whole-blood system, which provides a better model simulating human physiologic conditions. This system allows the study of the systemic effects of complement activation, unlike conventional assays that typically coculture cells with defined serum concentrations. Compared with huP, rearranged huP-3 elicited significantly improved cancer cell killing and monocyte-mediated phagocytosis, potentially due to increased C3 deposition on the cancer cell surface (9).

In summary, we present that the amplified complement activation led to delayed tumor growth and altered the TME in the context of pancreatic cancer model. Additionally, we have developed a novel membrane-bound oligomerized FP functional unit capable of eliciting potent complement activation. For translational studies, the rearranged mFP construct can be encapsulated into viral vectors or nanoparticles for targeted delivery in cancer therapy. Moreover, this application is not restricted to combination with α Gal but can also be applied with other antibody-based immunotherapies to enhance their therapeutic efficacy.

Figure 4.

Reconstructed huP showed an improved ability to induce complement activation. **A**, Schematic illustration of modified huP constructs. TM, transmembrane. **B**, Representative histogram showing the expression of modified huP on engineered Panc-1 (G⁻). **C**, C3 deposition on engineered Panc-1 cells expressing modified huP constructs after 2-hour incubation with 25% NHS. Data are presented in a representative histogram from one experiment, which was repeated once. **D** and **E**, C3 deposition on GGT1-expressing Panc-1(G⁻) engineered to express the original or modified huP-3 after 2-hour incubation with 25% NHS. EDTA (10 mmol/L) was added to the reaction to inactivate the complement as control. Data are presented in a representative histogram (**D**) and a bar plot (**E**) showing the individual mean fluorescence intensity (MFI) of technical triplicates with mean \pm SD from one experiment, which was repeated at least twice. The difference between groups under the NHS condition was compared using one-way ANOVA, followed by a Tukey multiple comparison test. **F–L**, Whole-blood loop assay for a systemic investigation of the functionality of huP-3. Gating strategies are presented in Supplementary Fig. S6. **F**, Schematic illustration of the experimental procedure. FC, flow cytometry. **G** and **H**, Representative counter plots (**G**) and quantification (**H**) of killed cancer cells. Background cell death was deducted. Data are presented as individual values from each donor with mean \pm SEM ($n = 5$). The difference between groups was analyzed using paired one-way ANOVA, followed by a Tukey multiple comparison test. **I–L**, Representative counter plots (**I** and **K**) and quantification (**J** and **L**) of the percentages of monocytes (CD14⁺ or CD16⁺) or neutrophils (CD15⁺CD16⁺) that phagocytosed cancer cells. Data are presented as individual values from each donor with mean \pm SEM ($n = 4$). The difference between groups was analyzed using paired one-way ANOVA, followed by a Tukey multiple comparison test. Key to statistics: *, $P < 0.05$; **, $P < 0.01$, and ***, $P < 0.001$.

Data Availability

All data generated or analyzed during this study are available from the corresponding author upon reasonable request. Unique materials used in this study, including plasmids and cell lines not commercially available, will be made available by the corresponding author upon request and completion of a standard material transfer agreement. The amino acid sequences for all mFP constructs generated in this study are publicly available in GenBank under accession numbers PX270894 – PX270901.

Authors' Disclosures

No disclosures were reported.

Authors' Contributions

M. Gao: Conceptualization, data curation, formal analysis, investigation, visualization, methodology, writing—original draft, writing—review and editing. **S. Kechagia:** Data curation. **M. Ramachandran:** Conceptualization, formal analysis, methodology, writing—review and editing. **V.A. Manivel:** Conceptualization, methodology, writing—review and editing. **N. Kadri:** Methodology, writing—review and editing. **B.-A. Cicortas:** Methodology, writing—review and editing. **C. Jin:**

Conceptualization, formal analysis, writing—review and editing. **D. Yu:** Conceptualization, supervision, funding acquisition, writing—review and editing.

Acknowledgments

We would like to express our sincere gratitude to Dr. Magnus Essand (Uppsala University, Sweden), Dr. Yang Chen (Lund University, Sweden), Dr. Nick Stub Laursen (Aarhus University, Denmark), and Dr. Dennis Vestergaard Pedersen (Aarhus University, Denmark) for their valuable discussions and input to the project. This work was supported by research grants from the Swedish Cancer Society (Cancerfonden) grant 22-2229Pj to D. Yu and the Swedish Childhood Cancer Fund (Barncancerfonden) grant PR2022-0105 to D. Yu. Portions of the manuscript were edited for grammar and style with the assistance of ChatGPT (OpenAI), and the accuracy and integrity were verified by the authors.

Note

Supplementary data for this article are available at Molecular Cancer Therapeutics Online (<http://mct.aacrjournals.org/>).

Received October 7, 2024; revised July 24, 2025; accepted October 24, 2025; posted first October 29, 2025.

References

- Galili U. Anti-Gal: an abundant human natural antibody of multiple pathogenesis and clinical benefits. *Immunology* 2013;140:1–11.
- Tanemura M, Miyoshi E, Nagano H, Eguchi H, Matsunami K, Taniyama K, et al. Cancer immunotherapy for pancreatic cancer utilizing α -gal epitope/natural anti-Gal antibody reaction. *World J Gastroenterol* 2015;21:11396–410.
- Albertini MR, Ranheim EA, Zuleger CL, Sondel PM, Hank JA, Bridges A, et al. Phase I study to evaluate toxicity and feasibility of intratumoral injection of α -gal glycolipids in patients with advanced melanoma. *Cancer Immunol Immunother* 2016;65:897–907.
- Galili U, Rachmilewitz EA, Peleg A, Flechner I. A unique natural human IgG antibody with anti-alpha-galactosyl specificity. *J Exp Med* 1984;160:1519–31.
- Galili U, Wigglesworth K, Abdel-Motal UM. Intratumoral injection of α -gal glycolipids induces xenograft-like destruction and conversion of lesions into endogenous vaccines. *J Immunol* 2007;178:4676–87.
- Galili U, Albertini MR, Sondel PM, Wigglesworth K, Sullivan M, Whalen GF. In situ conversion of melanoma lesions into autologous vaccine by intratumoral injections of α -gal glycolipids. *Cancers (Basel)* 2010;2:773–93.
- Taylor RP, Lindorfer MA. Cytotoxic mechanisms of immunotherapy: harnessing complement in the action of anti-tumor monoclonal antibodies. *Semin Immunol* 2016;28:309–16.
- Rogers LM, Veeramani S, Weiner GJ. Complement in monoclonal antibody therapy of cancer. *Immunol Res* 2014;59:203–10.
- Reis ES, Mastellos DC, Ricklin D, Mantovani A, Lambris JD. Complement in cancer: untangling an intricate relationship. *Nat Rev Immunol* 2018;18:5–18.
- Leshner AM, Nilsson B, Song W-C. Properdin in complement activation and tissue injury. *Mol Immunol* 2013;56:191–8.
- Michels MAHM, Volokhina EB, van de Kar NCAJ, van den Heuvel LPWJ. The role of properdin in complement-mediated renal diseases: a new player in complement-inhibiting therapy? *Pediatr Nephrol* 2019;34:1349–67.
- Pedersen DV, Gadeberg TAF, Thomas C, Wang Y, Joram N, Jensen RK, et al. Structural basis for properdin oligomerization and convertase stimulation in the human complement system. *Front Immunol* 2019;10:2007.
- Pedersen DV, Roumenina L, Jensen RK, Gadeberg TA, Marinuzzi C, Picard C, et al. Functional and structural insight into properdin control of complement alternative pathway amplification. *EMBO J* 2017;36:1084–99.
- Fearon DT, Austen KF. Properdin: binding to C3b and stabilization of the C3b-dependent C3 convertase. *J Exp Med* 1975;142:856–63.
- Medicus RG, Götze O, Müller-Eberhard HJ. Alternative pathway of complement: recruitment of precursor properdin by the labile C3/C5 convertase and the potentiation of the pathway. *J Exp Med* 1976;144:1076–93.
- Farries TC, Lachmann PJ, Harrison RA. Analysis of the interactions between properdin, the third component of complement (C3), and its physiological activation products. *Biochem J* 1988;252:47–54.
- Hourcade DE. The role of properdin in the assembly of the alternative pathway C3 convertases of complement. *J Biol Chem* 2006;281:2128–32.
- Pangburn MK. Analysis of the natural polymeric forms of human properdin and their functions in complement activation. *J Immunol* 1989;142:202–7.
- Blatt AZ, Pathan S, Ferreira VP. Properdin: a tightly regulated critical inflammatory modulator. *Immunol Rev* 2016;274:172–90.
- van den Bos RM, Pearce NM, Granneman J, Brondijk THC, Gros P. Insights into enhanced complement activation by structures of properdin and its complex with the C-terminal domain of C3b. *Front Immunol* 2019;10:2097.
- Muller M, Haghnejad V, Schaefer M, Gauchotte G, Caron B, Peyrin-Biroulet L, et al. The immune landscape of human pancreatic ductal carcinoma: key players, clinical implications, and challenges. *Cancers (Basel)* 2022;14:995.
- Tearle RG, Tange MJ, Zannettino ZL, Katerelos M, Shinkel TA, Van Denderen BJ, et al. The alpha-1,3-galactosyltransferase knockout mouse. Implications for xenotransplantation. *Transplantation* 1996;61:13–9.
- Lin Y-C, Chen B-M, Lu W-C, Su C-I, Prijovich ZM, Chung W-C, et al. The B7-1 cytoplasmic tail enhances intracellular transport and mammalian cell surface display of chimeric proteins in the absence of a linear ER export motif. *PLoS One* 2013;8:e75084.
- Harbury PB, Zhang T, Kim PS, Alber T. A switch between two-three-and four-stranded coiled coils in GCN4 leucine zipper mutants. *Science* 1993;262:1401–7.
- Hillerdal V, Nilsson B, Carlsson B, Eriksson F, Essand M. T cells engineered with a T cell receptor against the prostate antigen TARP specifically kill HLA-A2+ prostate and breast cancer cells. *Proc Natl Acad Sci U S A* 2012;109:15877–81.
- Rösner T, Lohse S, Peipp M, Valerius T, Derer S. Epidermal growth factor receptor targeting IgG3 triggers complement-mediated lysis of decay-accelerating factor expressing tumor cells through the alternative pathway amplification loop. *J Immunol* 2014;193:1485–95.
- Bergman I, Basse PH, Barmada MA, Griffin JA, Cheung NK. Comparison of in vitro antibody-targeted cytotoxicity using mouse, rat and human effectors. *Cancer Immunol Immunother* 2000;49:259–66.
- Ong GL, Mattes MJ. Mouse strains with typical mammalian levels of complement activity. *J Immunol Methods* 1989;125:147–58.
- Geis N, Zell S, Rutz R, Li W, Giese T, Mamidi S, et al. Inhibition of membrane complement inhibitor expression (CD46, CD55, CD59) by siRNA sensitizes tumor cells to complement attack in vitro. *Curr Cancer Drug Targets* 2010;10:922–31.
- Mamidi S, Cinci M, Hasmann M, Fehring V, Kirschfink M. Lipoplex mediated silencing of membrane regulators (CD46, CD55 and CD59) enhances complement-dependent anti-tumor activity of trastuzumab and pertuzumab. *Mol Oncol* 2013;7:580–94.
- Gong J, Larsson R, Ekdahl KN, Mollnes TE, Nilsson U, Nilsson B. Tubing loops as a model for cardiopulmonary bypass circuits: both the biomaterial and the blood-gas phase interfaces induce complement activation in an in vitro model. *J Clin Immunol* 1996;16:222–9.

32. Roumenina LT, Daugan MV, Petitprez F, Sautès-Fridman C, Fridman WH. Context-dependent roles of complement in cancer. *Nat Rev Cancer* 2019;19:698–715.
33. Vuagnat BB, Mach J-P, Le Doussal JM. Activation of the alternative pathway of human complement by autologous cells expressing transmembrane recombinant properdin. *Mol Immunol* 2000;37:467–78.
34. Pedersen DV, Rösner T, Hansen AG, Andersen KR, Thiel S, Andersen GR, et al. Recruitment of properdin by bi-specific nanobodies activates the alternative pathway of complement. *Mol Immunol* 2020;124:200–10.
35. Revel M, Daugan MV, Sautès-Fridman C, Fridman WH, Roumenina LT. Complement system: promoter or suppressor of cancer progression? *Antibodies* 2020;9:57.
36. Pittet MJ, Michielin O, Migliorini D. Clinical relevance of tumour-associated macrophages. *Nat Rev Clin Oncol* 2022;19:402–21.
37. Byrne KT, Betts CB, Mick R, Sivagnanam S, Bajor DL, Laheru DA, et al. Neoadjuvant selicrelumab, an agonist CD40 antibody, induces changes in the tumor microenvironment in patients with resectable pancreatic cancer. *Clin Cancer Res* 2021;27:4574–86.
38. Halama N, Zoernig I, Berthel A, Kahlert C, Klupp F, Suarez-Carmona M, et al. Tumoral immune cell exploitation in colorectal cancer metastases can be targeted effectively by anti-CCR5 therapy in cancer patients. *Cancer Cell* 2016;29:587–601.
39. Surace L, Lysenko V, Fontana AO, Cecconi V, Janssen H, Bicvic A, et al. Complement is a central mediator of radiotherapy-induced tumor-specific immunity and clinical response. *Immunity* 2015;42:767–77.
40. Böttcher JP, Reis e Sousa C. The role of type 1 conventional dendritic cells in cancer immunity. *Trends Cancer* 2018;4:784–92.
41. Wculek SK, Cueto FJ, Mujal AM, Melero I, Krummel MF, Sancho D. Dendritic cells in cancer immunology and immunotherapy. *Nat Rev Immunol* 2020;20:7–24.
42. Gebhardt T, Park SL, Parish IA. Stem-like exhausted and memory CD8⁺ T cells in cancer. *Nat Rev Cancer* 2023;23:780–98.
43. Galluzzi L, Smith KN, Liston A, Garg AD. The diversity of CD8⁺ T cell dysfunction in cancer and viral infection. *Nat Rev Immunol* 2025;25:1–18.
44. Brummelman J, Mazza EMC, Alvisi G, Colombo FS, Grilli A, Mikulak J, et al. High-dimensional single cell analysis identifies stem-like cytotoxic CD8⁺ T cells infiltrating human tumors. *J Exp Med* 2018;215:2520–35.
45. Held W, Siddiqui I, Schaeuble K, Speiser DE. Intratumoral CD8⁺ T cells with stem cell-like properties: implications for cancer immunotherapy. *Sci Transl Med* 2019;11:eaay6863.
46. Krishna S, Lowery FJ, Copeland AR, Bahadiroglu E, Mukherjee R, Jia L, et al. Stem-like CD8 T cells mediate response of adoptive cell immunotherapy against human cancer. *Science* 2020;370:1328–34.
47. Sade-Feldman M, Yizhak K, Bjorgaard SL, Ray JP, de Boer CG, Jenkins RW, et al. Defining T cell states associated with response to checkpoint immunotherapy in melanoma. *Cell* 2018;175:998–1013.e20.
48. Bhandarkar V, Dinter T, Spranger S. Architects of immunity: how dendritic cells shape CD8⁺ T cell fate in cancer. *Sci Immunol* 2025;10:eadf4726.
49. Waibl Polania J, Hoyt-Miggelbrink A, Tomaszewski WH, Wachsmuth LP, Lorrey SJ, Wilkinson DS, et al. Antigen presentation by tumor-associated macrophages drives T cells from a progenitor exhaustion state to terminal exhaustion. *Immunity* 2025;58:232–46.e6.
50. Uslu U, June CH. Beyond the blood: expanding CAR T cell therapy to solid tumors. *Nat Biotechnol* 2024;43:1–10.